Quantum Electronics **51** (10) 861–865 (2021)

INTERACTION OF EXTREME LIGHT FIELDS WITH MATTER https://doi.org/10.1070/QEL17601

Effect of electron–positron plasma production on the generation of a magnetic field in laser-plasma interactions

A.S. Samsonov, E.N. Nerush, I.Yu. Kostyukov

Abstract. **We consider the effect of electron–positron pair production on the generation of a quasi-stationary magnetic field in the interaction of an ultra-intense circularly polarised laser pulse with a thick plasma target. Full-scale three-dimensional numerical simulations by the particle-in-cell method performed taking into account quantum electrodynamic effects indicates a qualitative change in the generation of the magnetic field at a laser radiation intensity $I \gtrsim 10^{24}$ W cm^{-2}, which gives rise to a macroscopic number of electron–positron pairs. In this case, the amplitude of the magnetic field increases with an increase in the radiation intensity, whereas the amplitude of the magnetic field is hardly intensity-dependent when the effect of electron–positron pair production is neglected.**

Keywords: *inverse Faraday effect, electron–positron pair production, particle-in-cell simulation.*

It is believed that next-generation laser systems (ELI-NP [1], Apollon [2]) will enable experimental studies of laser-plasma interactions in the parameter range that delimits the classical and quantum regimes. One of the most significant features in this case is the radiation reaction force, which is able to largely determine the dynamics of particles. To date, numerical simulations have revealed a large number of configurations of laser-plasma interaction in which the radiation reaction leads to new effects, such as radiative trapping of particles [3–5], an increase in the amplitude of plasma waves [6, 7], new regimes of ion acceleration [8–12], effective absorption of a laser pulse [13–15], etc.

Despite the importance of the problem of the particle dynamics in an external electromagnetic field with radiation friction taken into account, in fact it has not yet been solved in the general case. Quasi-classical approximation can often be used, according to which the radiation reaction can be considered as an additional force in the equation of motion of a charged particle. In addition to the classical expression for the radiation reaction force written in the Landau–Lifshitz form, if necessary, one can take into account the quantum correction to the force associated with the cutoff of the synchrotron radiation spectrum at an energy equal to the energy of the radiating particle, which leads to a decrease in the total radiation power and can be accounted for the multiplication of the force by some factor $g < 1$ [16, 17]. This factor depends on the dynamic quantum electrodynamic (QED) particle parameter χ, which is equal to the ratio of the effective field in the particle's own reference frame to the Sauter–Schwinger critical field E_S [18]:

$$\chi = \frac{\gamma\sqrt{(\boldsymbol{E}+\boldsymbol{v}\times\boldsymbol{B})^2-(\boldsymbol{v}\boldsymbol{E})^2}}{E_S}, \tag{1}$$

where

$$E_S = \frac{m_e^2 c^3}{\hbar e} \approx 1.32\times 10^{18}\ \text{V m}^{-1}; \tag{2}$$

γ is the Lorentz factor of the particle; $\boldsymbol{v}$ is the particle velocity; $\boldsymbol{E}$ and $\boldsymbol{B}$ are the electric and magnetic fields, respectively; m_e is the electron mass; c is the speed of light; $\hbar$ is Planck's constant; and $e > 0$ is the electron charge magnitude.

In this work, we study the absorption of the angular momentum of high-intensity circularly polarised laser radiation by a plasma (also called the inverse Faraday effect), which leads to the generation of a quasi-stationary magnetic field [19–28]. In the presence of additional interaction, which can be associated, for example, with plasma fields [26], interparticle collisions [27] or radiation reaction [28], the electromagnetic angular momentum carried by a circularly polarised laser pulse can be transferred to plasma electrons. In this case, the electrons acquire a torque that gives rise to an azimuthal current and, therefore, to an axial magnetic field. In our work, it is the radiation reaction that is considered as the dissipative force. In this case, the inverse Faraday effect can be qualitatively described from the quantum point of view: In the course of nonlinear Compton scattering, an electron absorbs $N \gg 1$ laser photons with a total orbital angular momentum $N\hbar$ and radiates one high-energy photon with an orbital angular momentum $\hbar$, and the difference in angular momentum $(N-1)\hbar$ is converted into the orbital motion of the electron.

Analytical models were proposed in [28, 29] that describe this process both in the classical and quantum regimes. In the latter case, the semiclassical approach considered above was used, which made it possible to calculate a decrease in the efficiency of generation of the magnetic field and, therefore, its maximum amplitude due to the factor g. However, when the radiation intensity is as high as 10^{24} W cm^{-2}, the interaction occurs in the regime when each photon radiated by the electron can carry away a significant part of its energy. Together with the fact that the radiation is stochastic in nature, this

A.S. Samsonov, E.N. Nerush Institute of Applied Physics, Russian Academy of Sciences, ul. Ulyanova 46, 603950 Nizhny Novgorod, Russia; e-mail: asams@ipfran.ru;
I.Yu. Kostyukov Institute of Applied Physics, Russian Academy of Sciences, ul. Ulyanova 46, 603950 Nizhny Novgorod, Russia; National Research Nuclear University MEPhI, Kashiskoe shosse 31, 115409 Moscow, Russia

Received 18 June 2021
Kvantovaya Elektronika **51** (10) 861–865 (2021)
Translated by E.N. Ragozin

leads to a significant spread of the parameters of particles, for example, of the energy relative to the mean value, which is described by the semiclassical approach. It is evident that the angular momentum absorption efficiency calculated from some averaged particle characteristics, in the general case, does not coincide with the coefficient obtained as a result of averaging the efficiency calculated for each individual particle.

At such intensities, an equally important QED effect is the decay of gamma photons radiated by electrons into electron–positron pairs (the Breit–Wheeler process) [30]. Recent studies have shown that this process can significantly modify the interaction of laser radiation with matter [31–37]. In this paper, we consider the so far separately unexplored problem of the influence of secondary particles produced as a result of QED processes on the generation of magnetic fields during the interaction of high-power laser radiation with plasmas. Due to the complexity of the phenomenon, the main research tool in our work was numerical simulation.

Full-scale three-dimensional numerical simulations were performed with the QUILL code [38], which implements the particle-in-cell method and the Monte Carlo method for describing quantum processes. The initial field distribution of the laser pulse was set in such a way that at the instant the centre of the laser pulse crossed the plane $x = 0$, which coincided with the left boundary of the target, it was of the form:

$$\boldsymbol{a}(x,y,z) = a_0\left[\boldsymbol{y}_0\cos\left(\frac{\omega_L x}{c}\right) + \boldsymbol{z}_0\sin\left(\frac{\omega_L x}{c}\right)\right]$$

$$\times\cos^2\left(\frac{\pi}{2}\frac{x^4}{\sigma_x^4}\right)\exp(-r^n/r_0^n), \qquad (3)$$

where $r^2 = y^2 + z^2$; $a_0 = eE/(m_e c\omega_L)$ is the dimensionless pulse amplitude; $\omega_L = 2\pi c/\lambda$; $\lambda = 1$ μm is the radiation wavelength; $\sigma_x = c/\tau$; $\tau = 10$ fs is the pulse duration; $r_0 = 3.2$ μm is the beam waist radius; and $n = 2$ for the Gaussian envelope and $n = 4$ for the super-Gaussian one. The simulation results suggest that the transverse envelope of the laser pulse does not significantly affect the generation of the magnetic field and the electron–positron pair production. The grid steps in space are $\Delta x = 0.015\lambda$ and $\Delta y = \Delta z = 0.25\lambda$, and the time step is $\Delta t = 0.01\lambda/c$. In the target region ($0 < x < d$, $-10\lambda < y, z < 10\lambda$, where d is the target thickness), two particles, an electron and an ion, were initialised to simulate a completely ionised plasma with a density n_e in each cell. The size of the simulation domain was 35λ in the x coordinate and 25λ in the y and z coordinates.

Initially, we determined the parameters of the plasma target for which the amplitude of the generated magnetic field reached its maximum, in the case when the decay of photons into electron–positron pairs was not taken into account. It was found that the optimal parameters of the laser radiation and the target are in the relation $a_0 = kn_e$, where n_e is the electron density of the target measured in units of nonrelativistic critical density $n_{cr} = m_e\omega_L^2/(4\pi e^2)$, and k is a numerical coefficient of the order of 10. It was found that the laser pulse is greatest absorbed by the target rather than reflected from it when this relation is fulfilled (Fig. 1). The presence of a maximum in the dependence of the absorption coefficient on the plasma density can be attributed to the fact that at low plasma densities it is impossible to generate sufficiently high currents to absorb the laser pulse, and therefore it passes through the target with hardly any absorption and, when interacting with supercritical plasma, the laser pulse is reflected without being strongly absorbed. In the intermediate region corresponding to a near-critical plasma, that is, to a plasma with a density $n_e \approx 0.1a_0n_{cr}$, the laser pulse undergoes strong absorption.

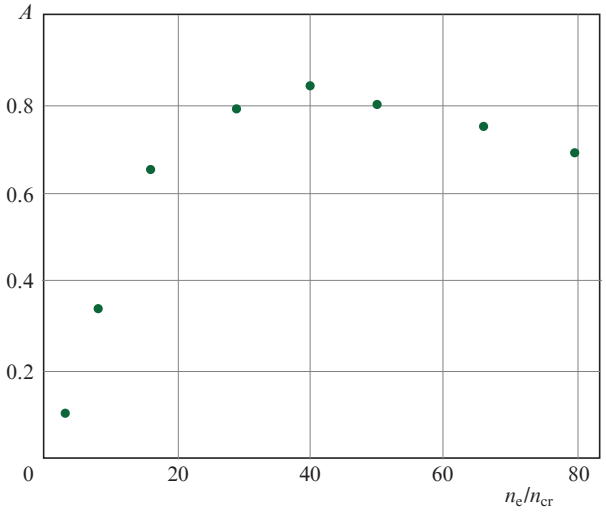

Figure 1. Coefficient of laser pulse absorption by a thick target (d = 10 μm) as a function of the electron density calculated as the difference from unity of the ratio of the final laser pulse energy to the initial one. In the simulation, the laser field amplitude $a_0 = 500$ was used, and the decay of gamma photons into electron–positron pairs was not taken into account. The maximum absorption coefficient is reached for $n_e = 40n_{cr} = a_0n_{cr}/12.5$.

Next, we carried out a series of numerical simulations with different parameters of the laser pulse and target: The laser pulse amplitude a_0 varied in the range 250–2500, which corresponded to the intensity range 7×10^{22}–7×10^{24} W cm^{-2}, the target density satisfied the condition $a_0 = 12.5n_e$, and the target thickness was $d = 10$ μm. Each simulation was performed twice: with and without the decay of photons into electron–positron pairs. An example of the distribution of the quasi-stationary magnetic field is shown in Fig. 2.

An analysis of the simulation data indicates the existence of different laser pulse–target interaction regimes. For a dimensionless laser pulse field amplitude $a_0 \lesssim 750$, an increase in the laser pulse intensity leads to an increase in the amplitude of the generated magnetic field, while taking into account the decay of hard photons into electron–positron pairs has hardly any effect on the generation of the magnetic field (Fig. 3). This can be explained by the fact that the angular momentum of the laser pulse is zero on its symmetry axis, and the angular momentum is at its maximum in the region of the maximum of the radial derivative of the field intensity, that is, at the edges of the laser pulse. In this case, the decay of hard photons is determined by the magnitude of the field, and the absorption of the angular momentum is determined by the magnitude of the radial derivative of the field. Thus, these processes are spatially separated and therefore hardly affect each other.

Without taking into account the decay of gamma photons into electron–positron pairs, for a dimensionless laser pulse field amplitude $a_0 \gtrsim 750$ the simulations showed a decrease in the efficiency of magnetic field generation and the attainment of the limiting value of the magnetic field amplitude for a

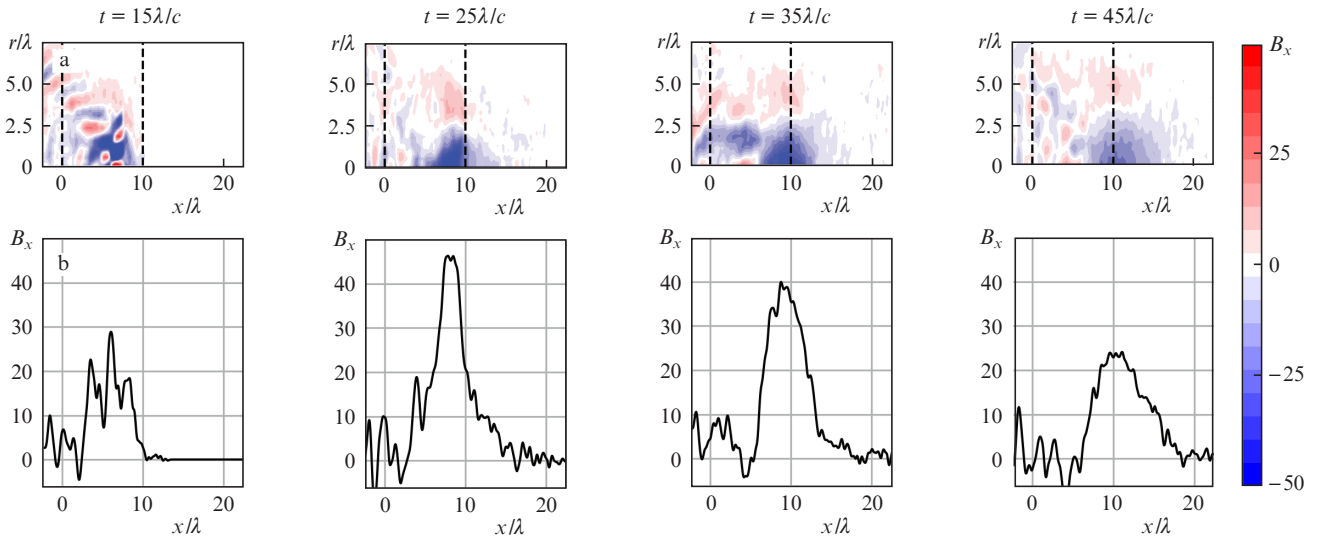

Figure 2. (Colour online) Distributions of the longitudinal quasi-stationary magnetic field B_x obtained by simulations taking into account gamma photon decay into electron–positron pairs for a laser field amplitude $a_0 = 1500$ at different points in time (a) in the plane 'longitudinal coordinate x – radius r' and (b) on the x axis. Vertical dashed lines indicate target boundaries. The magnetic field is normalised to the quantity $m_e c\omega_L/e \approx 0.1$ GG for $\lambda = 1$ μm. By the point in time $t = 15\lambda/c$, the laser field in the target region is practically absent due to its absorption and partial reflection.

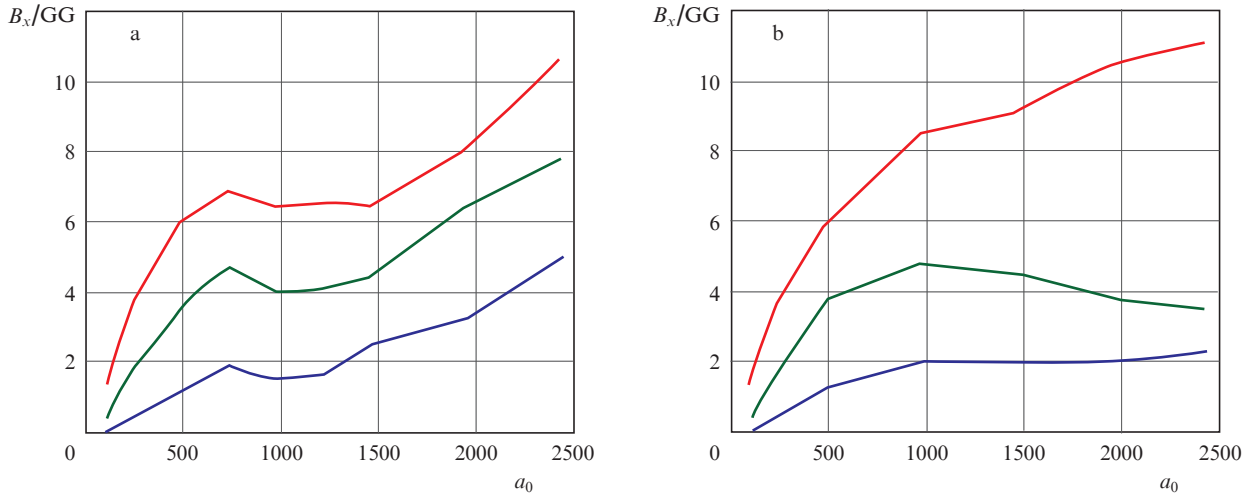

Figure 3. (Colour online) Dependences of the amplitude of the generated magnetic field on the amplitude of the laser pulse in the simulation (a) with and (b) without electron–positron pair production. Red curves: the maximum value of the longitudinal magnetic field; blue (green) curves: the average value of the magnetic field, calculated by formula (4) for $m = 1$ (0).

radiation intensity $I \approx 10^{24}$ W cm^{-2}, in accordance with the semiclassical description developed in [29]. Taking into account the production of electron–positron pairs, this dependence changes qualitatively. For a laser pulse field amplitude of $750 \lesssim a_0 \lesssim 1250$, which corresponds to the intensity at which a macroscopic number of pairs begins to emerge (their density reaches a maximum of 1.3×10^{24} cm$^{-3} \approx 9.5 n_e$ for $a_0 = 1000$), a decrease in the magnetic field amplitude is observed compared to the case when the simulation is performed without photon decay taken into account. When simulating in the indicated range of laser pulse amplitudes, electron–positron pairs are formed mainly behind the rear boundary of the target and near the axis of the laser pulse (Fig. 4b), which, possibly, is one of the reasons for a decrease in the efficiency of magnetic field generation. However, the specific mechanism due to which this happens is still unknown, and this issue calls for additional investigation.

With a further increase in the laser pulse amplitude ($a_0 \gtrsim 1250$), the direct dependence of the magnetic field amplitude on it is restored. In this case, the electron–positron plasma is produced inside the channel devoid of target particles and formed in the process of hole-boring, while its density becomes comparable to the target density and reaches a maximum value of 3.2×10^{25} cm$^{-3} \approx 94.7 n_e$ for $a_0 = 2500$ (Fig. 4c). In this regime, the electron–positron plasma, apparently, also participates in the absorption of the angular momentum of laser radiation and, consequently, in the generation of the magnetic field. This leads to the fact that the amplitude of the

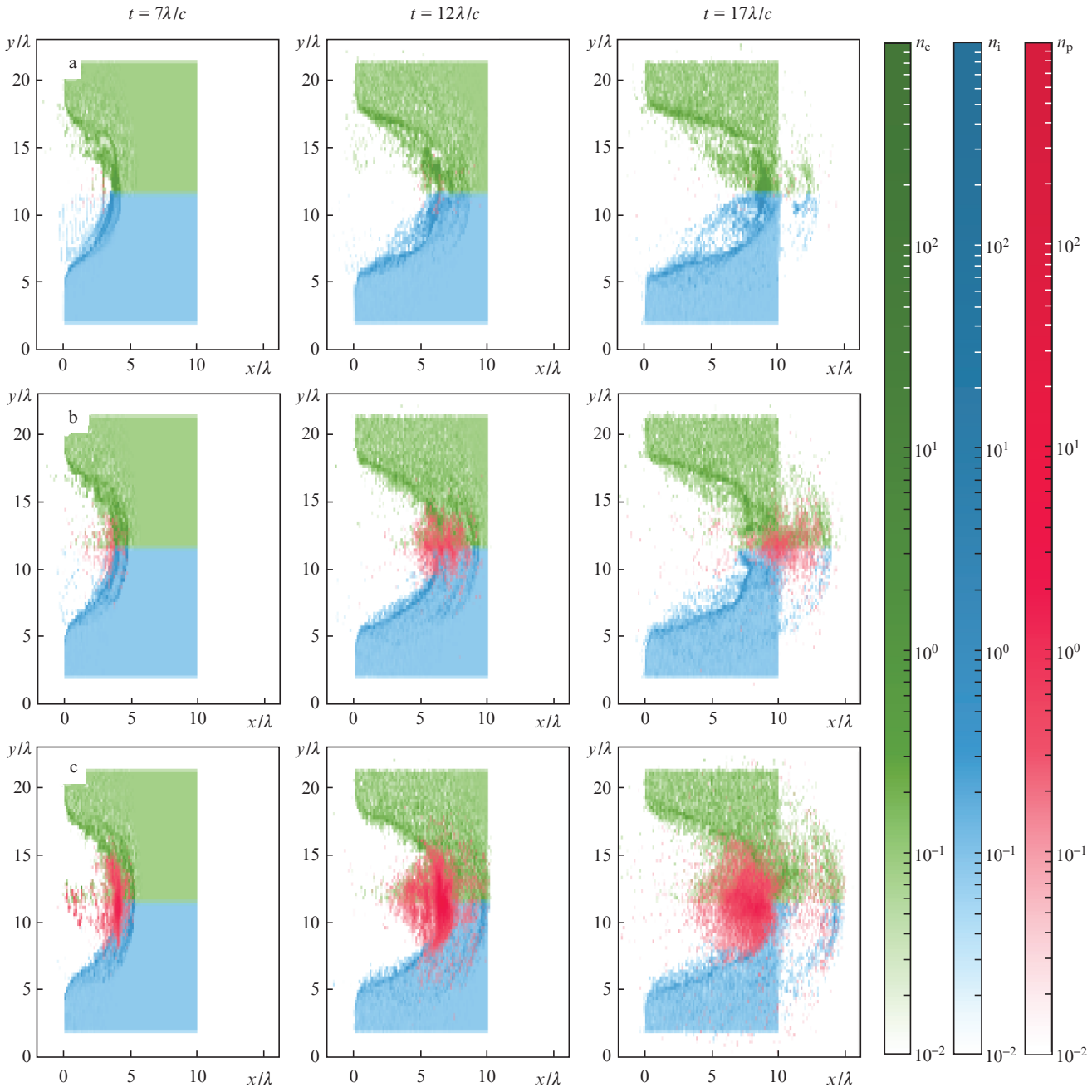

Figure 4. (Colour online) Electron–positron plasma structures produced during the interaction of laser radiation with a thick target for a_0 = (a) 500, (b) 1000, and (c) 2500. The distributions of electron (n_e; green), ion (n_i; blue), and positron (n_p; red) densities normalised to the relativistic critical density $a_0 n_{cr}$ are presented in the xy plane at the point in time $t = 20\lambda/c$. The maximum densities of the electron–positron plasma were 1.1×10^{23} cm^{-3} $\approx 1.7 n_e$, 1.3×10^{24} cm^{-3} $\approx 9.5 n_e$, and 3.2×10^{25} cm^{-3} $\approx 94.7 n_e$ for $a_0 = 500$, 1000, and 2500, respectively.

magnetic field does not saturate, as in the case when pair production is not taken into account, but continues to grow with increasing radiation intensity. Interestingly, in this regime the electron–positron plasma is 'trapped' by the laser pulse, that is, the laser pulse does not push it in the transverse direction by the ponderomotive force, in contrast to the target plasma. As noted above, the effect of radiative trapping and a significant change in the macroscopic dynamics of particles when interacting with laser radiation, whose intensity is close to the threshold for the onset of the production of a large number of electron–positron pairs from photons, is observed in some other configurations of laser-plasma interaction.

It should be noted that there are several ways to determine the amplitude of the magnetic field from numerical simulation data. In particular, we used three different methods according to which the dependence of the magnetic field amplitude on the laser pulse intensity repeats the one described above. The first method corresponds to the red curve in Fig. 3 and involves calculating the minimum (due to the chosen polarisation of the laser pulse, the generated magnetic field is directed oppositely to the x axis) of the magnetic field component B_x over the entire region and over the simulation time. The second and third methods correspond to the green and blue curves in Fig. 3 and involve calculating, over the simula-

tion time, the minimum of the average component value $\langle B_x \rangle$, calculated by the formula

$$\langle B_x \rangle = -\frac{m+1}{r_{\max}^{m+1} x_{\max}} \int_0^{x_{\max}} \int_0^{r_{\max}} B_x(x,r) r^m \mathrm{d}r\mathrm{d}x, \qquad (4)$$

where $m = 0, 1$; $x_{\max} = 2d$; and $r_{\max} = 1.5r_0$.

Thus, we have discovered an effect consisting in a qualitative change in the generation of a quasi-stationary magnetic field during the interaction of circularly polarised laser radiation with a thick plasma target when the radiation intensity exceeds 10^{24} W cm^{-2}, which is associated with the production of a macroscopic number of electron–positron pairs. The production of pairs has the effect that the amplitude of the magnetic field increases with increasing intensity of laser radiation. When the pair production is neglected, the amplitude of the magnetic field reaches a certain limiting value and does not increase at an intensity above 10^{24} W cm^{-2}. The result obtained is an important addition to the qualitative picture of this process. An explanation and an analytical description of the mechanism of magnetic field generation with allowance for the production of secondary particles is planned to be given in future publications.

Acknowledgements. This work was supported by the Russian Science Foundation (Grant No. 20-12-00077).

References

1. The Extreme Light Infrastructure (ELI); http://www.eli-laser.eu.
2. https://portail.polytechnique.edu/luli/en/cilex-apollon/apollon.
3. Gonoskov A., Gonoskov I., Harvey C., Ilderton A., Kim A., Marklund M., Mourou G., Sergeev A. *Phys. Rev. Lett*., **111**, 60404 (2013).
4. Ji L.L., Pukhov A., Kostyukov I.Yu., Shen B.F., Akli K. *Phys. Rev. Lett*., **112**, 145003 (2014).
5. Ji L.L., Pukhov A., Nerush E.N., Kostyukov I.Yu., Shen B.F., Akli K. *Phys. Plasmas*, **21**, 023109 (2014).
6. Gelfer E.G., Elkina N.V., Fedotov A.M. *Sci. Rep*., **8**, 6478 (2018).
7. Gelfer E.G., Fedotov A.M., Weber S. *Plasma Phys. Control. Fusion*, **60**, 064005 (2018).
8. Tamburini M., Pegoraro F., Piazza A.D., Keitel C.H., Macchi A. *New J. Phys*., **12**, 123005 (2010).
9. Tamburini M., Liseykina T.V., Pegoraro F., Macchi A. *Phys. Rev. E*, **85**, 016407 (2012).
10. Capdessus R., d'Humières E., Tikhonchuk V.T. *Phys. Rev. E*, **86**, 036401 (2012).
11. Capdessus R., McKenna P. *Phys. Rev. E*, **91**, 053105 (2015).
12. Nerush E.N., Kostyukov I.Yu. *Plasma Phys. Control. Fusion*, **57**, 035007 (2015).
13. Grismayer T., Vranic M., Martins J.L., Fonseca R.A., Silva L.O. *Phys. Plasmas*, **23**, 056706 (2016).
14. Savin A.F., Ross A.J., Aboushelbaya R., Mayr M.W., Spiers B., Wang R.H., Norreys P.A. *Sci. Rep*., **9**, 8956 (2019).
15. Popruzhenko S.V., Liseykina T.V., Macchi A. *New J. Phys*., **21**, 033009 (2019).
16. Ritus V.I. *Trudy FIAN*, **111**, 5 (1979).
17. Baier V.N., Katkov V.M., Strakhovenko V.M. *Elektromagnitnye protsessy pri vysokoi energii v orientirovannykh monokristallakh* (Electromagnetic Processes at High Energy in Oriented Single Crystals) (Novosibirsk: Nauka. Siberian Branch, 1989).
18. Berestetskii V.B., Lifshitz E.M., Pitaevskii L.P. *Kvantovaya elektrodinamika* (Quantum Electrodynamics) (Moscow: Nauka, 1989).
19. Pitaevskii L.P. *Sov. Phys. JETP*, **12**, 1008 (1961) [*Zh. Eksp. Teor. Fiz*., **39** (5), 1450 (1961)].
20. Steiger A.D., Woods C.H. *Phys. Rev. A*, **5**, 1467 (1972).
21. Abdullaev A.Sh., Frolov A.A. *Sov. Phys. JETP*, **54**, 493 (1981) [*Zh. Eksp. Teor. Fiz*., **81** (3) 917 (1981)].
22. Bychenkov V.Yu., Demin V.Yu., Tikhonchuk V.T. *J. Exp. Theor. Phys*., **78**, 62 (1994) [*Zh. Eksp. Teor. Fiz*., **105** (1), 188 (1994)].
23. Haines M.G. *Phys. Rev. Lett.*, **87**, 135005 (2001).
24. Sheng Z.-M., Meyer-ter-Vehn J. *Phys. Rev. E*, **54**, 1833 (1996).
25. Berezhiani V.I., Mahajan S.M., Shatashvili N.L. *Phys. Rev. E*, **55**, 995 (1997).
26. Kostyukov I.Y., Shvets G., Fisch N.J., Rax J.-M. *Phys. Plasmas*, **9**, 636 (2002).
27. Shvets G., Fisch N.J., Rax J.-M. *Phys. Rev. E*, **65**, 046403 (2002).
28. Liseykina T.V., Popruzhenko S.V., Macchi A. *New J. Phys*., **18**, 072001 (2016).
29. Liseykina T.V., Macchi A., Popruzhenko S.V. *Eur. Phys. J. Plus*, **136**, 1 (2021).
30. Breit G., Wheeler J.A. *Phys. Rev*., **46**, 1087 (1934).
31. Ridgers C.P., Brady C.S., Duclous R., Kirk J.G., Bennett K., Arber T.D., Robinson A.P.L., Bell A.R. *Phys. Rev. Lett*., **108**, 165006 (2012).
32. Kirk J.G., Bell A.R., Ridgers C.P. *Plasma Phys. Control. Fusion*, **55**, 095016 (2013).
33. Kostyukov I.Yu., Nerush E.N. *Phys. Plasmas*, **23**, 093119 (2016).
34. Yuan T., Yu J.Y., Liu W.Y., Weng S.M., Yuan X.H., Luo W., Chen M., Sheng Z.M., Zhang J. *Plasma Phys. Control. Fusion*, **60**, 065003 (2018).
35. Lu Y., Yu T.-P., Hu L.-X., Ge Z.-Y., Wang W.-Q., Liu J.-X., Liu K., Yin Y., Shao F.-Q. *Plasma Phys. Control. Fusion,* **60**, 125008 (2018).
36. Samsonov A.S., Nerush E.N., Kostyukov I.Yu. *Sci. Rep*., **9**, 11133 (2019).
37. Samsonov A.S., Kostyukov I.Yu., Nerush E.N. *Matter Radiat. Extremes*, **6**, 034401 (2021).
38. QUILL code; https://github.com/QUILL-PIC/Quill.